Check for updates

New insights into Li distribution in the superionic argyrodite Li_6PS_5Cl†

Enyue Zhao, [ID] [ab] Lunhua He, [bc] Zhigang Zhang, [b] Jean-Marie Doux, [ID] [a] Darren H. S. Tan, [a] Erik A. Wu, [a] Grayson Deysher, [d] Yu-Ting Chen, [d] Jinkui Zhao, [b] Fangwei Wang [bc] and Ying Shirley Meng [ID] *[ade]

By using temperature-dependent neutron powder diffraction combined with maximum entropy method analysis, a previously unreported Li lattice site was discovered in the argyrodite Li_6PS_5Cl solid-state electrolyte. This new finding enables a more complete description of the Li diffusion model in argyrodites, providing structural guidance for designing novel high-conductivity solid-state electrolytes.

All-solid-state lithium batteries (ASSLBs) have attracted much attention recently, due to their prospects for higher safety, improved thermal stability, as well as potentially higher energy densities.[1–3] The solid-state electrolyte (SSE), as a critical component of ASSLBs, affects the battery's overall performance; gaining a deeper understanding on its physical and electrochemical properties is vital. Various SSEs including polymers, oxides, halides, and sulfides, have been developed and applied in ASSLBs in the literature.[4] Identifying new SSEs that possess high ionic conductivity and adequate chemical and electrochemical stability is a very active research area. For sulfide-based SSEs, significant progress has been made on improving their ionic conductivity, with conductivity values now similar to liquid electrolytes (e.g., the Li argyrodites $Li_{6+x}P_{1-x}Ge_xS_5I$ and $Li_{6+x}Sb_{1-x}Si_xS_5I$).[5,6] However, ionic conductivity alone is insufficient to evaluate SSEs, properties such as electrochemical stability, low electronic conductivity, as well as interfacial passivation are also vital for good cell performance. To this end, Li argyrodite Li_6PS_5X (X = halogens) are considered to be a particularly promising family of SSEs as they have been shown to meet these requirements.[7–9]

The argyrodite Li_6PS_5X structure can be represented by a cubic close-packed lattice formed by the X^- anions (Wyckoff $4a$), in which S^{2-} ions occupy half of the tetrahedral voids (Wyckoff $4d$) while PS_4^{3-} units occupy the octahedral sites (S and P on Wyckoff $16e$ and $4b$, respectively).[7] A tetrahedrally close-packed lattice can be constructed through this three-dimensional spatial distribution of anions (i.e., X and S) at the $4a$, $4d$, and $16e$ sites. The center of these tetrahedra are interstitial sites which can accommodate either lattice cations (i.e., P) or mobile lithium ions. Six distinct tetrahedral types (types 0–5) were described by Deiseroth et al. in this argyrodite structure (Fig. S1, ESI†).[10] The tetrahedra site occupied by P is defined as type 0 and the remaining tetrahedra available to potentially accommodate Li are classified into five types (types 1–5) based on the number of corners or edges each tetrahedron shares with neighboring PS_4^{3-} units.[10]

Previous neutron diffraction studies on Li_6PS_5X have assigned lithium ions as primarily occupying the type 5 (T5) site (Wyckoff $48h$), with observations of a "smeared out" lithium density distributed at the shared face of adjacent T5 tetrahedral pairs (Wyckoff $24g$, denoted as type 5a site by Deiseroth et al.).[9,10] The conventional Li diffusion model in Li_6PS_5X considers only T5 and type 5a (T5a) sites, which together form a cage-like geometry centered around the nominal S^{2-} sites (Wyckoff $4d$). There are three jump models between T5 and T5a sites, enabling lithium-ion migration in Li_6PS_5X.[11,12] Specifically, doublet jumps ($48h–24g–48h$) consist of localized Li migration between face-sharing T5 tetrahedra via the T5a position. Intra-cage jumps ($48h–48h$) represent short–range lithium migration between pairs of non-face-sharing T5 tetrahedra within the same $4d$-centered cage. Finally, inter-cage jumps consist of long–range lithium migration between T5 positions associated with different $4d$-centered cages. This three-jump model (doublet, intra-cage, and inter-cage) has been widely used to describe the lithium diffusion in Li_6PS_5X and related Li argyrodites.[9,10,13–16]

[a] Department of NanoEngineering, University of California San Diego, La Jolla, CA 92093, USA. E-mail: shirleymeng@ucsd.edu

[b] Songshan Lake Materials Laboratory, Dongguan 523808, P. R. China

[c] Spallation Neutron Source Science Center, Dongguan, 523803, P. R. China

[d] Program of Materials Science and Engineering, University of California San Diego, La Jolla, CA 92093, USA

[e] Sustainable Power & Energy Center (SPEC), University of California San Diego, La Jolla, CA 92093, USA

Since the T5 tetrahedra cannot form connected face-sharing pairs, the long–range inter-cage Li migration requires Li to pass through other (*i.e.*, non-type-5) tetrahedra. Therefore, a description of lithium diffusion that only considers the T5 and T5a sites is incomplete. Previous bond-valence calculations and molecular dynamics simulations have highlighted the role of non-type-5 positions in the Li diffusion path in the argyrodite structure.[17–20] Recent experimental studies have also found that there is Li occupation of non-type-5 sites in the Li argyrodites with Li stoichiometry $x_{Li} > 6$, and this Li-excess stoichiometry was reported to be the direct cause of the non-type-5 site occupation.[5,6,21] In addition, the Li occupation of the type 2 position (T2, Wyckoff 48h), was also experimentally confirmed in $x_{Li} = 6$ systems (Li$_6$PS$_5$X) *via* neutron diffraction.[22] Meanwhile, first-principles molecular dynamics simulations have predicted that the type 4 (T4, Wyckoff 16e) position may also be occupied in the same system.[17] As noted above, while the basic Li substructure in Li$_6$PS$_5$X has been well clarified, an in-depth quantification of Li distribution is still needed to define a more complete Li diffusion model. This will facilitate further optimization of argyrodite compounds from the perspective of Li sublattice structure and provide structural guidance for the design of new high ionic conductivity SSEs.[6,23]

Herein, the high-conductivity Li argyrodite Li$_6$PS$_5$Cl (in which only Li has a negative neutron coherent-scattering length, Table S1, ESI†) was selected as the model compound, and temperature-dependent neutron powder diffraction (NPD) combined with maximum entropy method (MEM) analysis was employed to study the Li distribution in the argyrodite lattice. MEM is useful to modify the structural models employed in Rietveld analysis and determine the distribution of the nuclear density (*i.e.*, coherent-scattering length) from NPD data.[24–26] Since MEM can estimate the structure factors of high-Q reflections that have not been measured experimentally, the termination effect is less serious in MEM analysis than in Fourier synthesis.[25] In addition, compared with X-ray or electron-based methods, neutron is more sensitive to lithium.[27–29] Combined with MEM analysis, NPD can therefore provide insights on the Li sublattice structure beyond the traditional Rietveld structure analysis. We demonstrate that, other than Li occupation of T5 and T2 positions, there is a small fraction of Li ions located around the type 1 site (denoted as Type 1x site or T1x, Wyckoff 48h) in Li$_6$PS$_5$Cl, which has not been previously observed. In light of the observed Li location on additional sites, a new possible Li conduction pathway is proposed, which enriches the description of the ionic diffusion mechanism, and completes the Li diffusion model for the Li argyrodite SSEs.

The typical unit cell structure of Li$_6$PS$_5$Cl is shown in Fig. 1a. Contrary to the anion-ordered structure of Li$_6$PS$_5$I, in which I$^-$ and S^{2-} anions occupy distinct crystallographic sites, Li$_6$PS$_5$Cl adopts an anion-disordered structure where the Cl$^-$ and S^{2-} anions are significantly disordered across the Wyckoff 4a and 4d sites.[7,9] The degree of anion disorder in Li$_6$PS$_5$Cl is closely associated with the Li-ion concentration as well as the synthesis process.[7,9] Both theoretical and experimental studies have suggested that the anion disorder originates from the
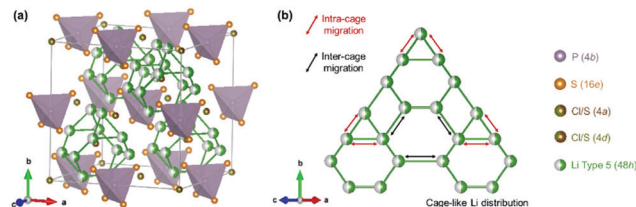
Fig. 1 (a) The crystal structure of Li$_6$PS$_5$Cl, in which Cl$^-$ (Wyckoff 4a) forms a face-centered cubic lattice with S^{2-} (Wyckoff 4d) in half of the tetrahedral voids and PS$_4^{3-}$ units (P on Wyckoff 4b, S on Wyckoff 16e) in the octahedral sites. In this structure, S^{2-}/Cl$^-$ shows significant site disorder. Type 5 Li position (Wyckoff 48h) form four localized cages in a unit cell and enable the short–range and long–range Li migration. (b) Schematic structure of intra-cage (short–range) Li migration (48h–48h) and inter-cage (long–range) Li migration among three cages in a unit cell.

similar ionic radii of S^{2-} (1.84 Å) and Cl$^-$ (1.81 Å).[7,9] It was proposed that the site disorder in the argyrodite structures has a strong effect on their lithium diffusion properties. The site disorder between S^{2-} and Cl$^-$ can decrease the Li-ion transport barrier, leading to the much higher room-temperature ionic conductivity ($\sim$2 mS cm^{-1}) in Li$_6$PS$_5$Cl compared to Li$_6$PS$_5$I where anions (*i.e.*, S^{2-} and I$^-$) occupy distinct ordered sites.[9,17]

The superior lithium migration properties in the argyrodite Li$_6$PS$_5$Cl can also be closely correlated with its unique Li substructure. As previously mentioned, only one crystallographic position, T5, is conventionally considered when discussing Li distribution in Li$_6$PS$_5$Cl.[9,10] This T5 position can form a cage-like local polyhedra (Fig. 1a), enabling both intra-cage and inter-cage lithium-ion hopping processes (Fig. 1b). In order to further revisit the Li substructure and deepen the understanding of Li diffusion mechanisms within the Li$_6$PS$_5$Cl argyrodite lattice, high-resolution temperature-dependent NPD data (at 5, 300, and 550 K) were collected. Since the Li distribution in the argyrodite lattice is temperature-dependent, the low-temperature measurement can effectively freeze the motion of lithium ions, resolving subtle changes of the Li substructure (Li occupancies) that may be hidden by the fast Li ion-conducting nature of Li$_6$PS$_5$Cl. At extremely low temperatures (*e.g.*, 5 K), lithium ions stabilize in the lowest-energy sites, and may then move to the other sites along the diffusion pathways when temperature increases (*e.g.*, 300 and 550 K). The temperature dependence of the Li distribution can help provide critical insights into the underlying potential energy surface that dictates the viability of competing Li-ion migration pathways.[17,22]

Fig. 2 shows the Rietveld refinement results of the neutron diffraction data at 300 K when considering only the T5 Li position in the refined structure model. A relatively good agreement between the calculated diffraction pattern and the experimental data was observed (R_{wp} = 2.20%), the detailed refinement structure parameters are presented in Table S5 (ESI†). It appears that the diffraction patterns can be well described by the cubic structure using the $F\bar{4}3m$ space group. The obtained site disorder between S^{2-} and Cl$^-$, defined as the total fraction of Cl$^-$ on the S^{2-} site, is 54% (Table S5, ESI†). Based on the Rietveld refinement results, MEM analysis was used to explore the Li nuclear density distribution in the Li$_6$PS$_5$Cl lattice. Since only Li has a negative neutron coherent-scattering
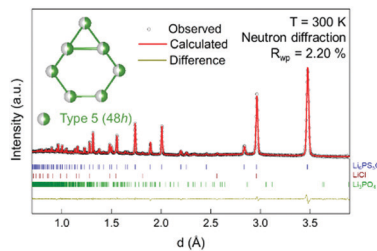
Fig. 2 NPD data collected at 300 K and Rietveld refinement results based on Li sublattice structure model (inset) with only type 5 Li positions. Positions of the Bragg reflections are shown as blue vertical ticks for Li_6PS_5Cl, red ticks for LiCl, and green ticks for Li_3PO_4. Only small fractions of the impurity phases LiCl (0.48 wt%) and Li_3PO_4 (1.06 wt%) were observed.

Fig. 4 NPD data of Li_6PS_5Cl collected at (a) 5 K, (b) 300 K and (c) 550 K, as well as corresponding Rietveld refinement results based on different Li sublattice structure models (inset). Other than the T5 and T2 Li positions, T1x Li was observed in Li_6PS_5Cl at 300 K and 550 K, and the T5a Li position was also found at 550 K. (d) The Li distribution breakdown in Li_6PS_5Cl as a function of temperature.

length in Li_6PS_5Cl, the Li nuclear density can easily be differentiated from the nuclear densities of other atoms. Notably, besides the Li nuclear density located at the T5 position, some unexpected Li nuclear density was located at both the T2 position and around the T1 position (denoted as T1x; Fig. 3). While the T2 Li position in the Li_6PS_5Cl lattice has been previously reported, the Li position located at T1x has not. In order to further confirm that the Li nuclear density located at the T1x position is not merely transient, the refinement structure model was modified to consider Li occupation not only at the T5 site, but also the T2 and T1x sites; then, Rietveld refinement was performed again for the NPD data collected at 300 K (Fig. 4b). It was found that ∼ 16% and ∼ 7% of the total lithium atoms in the unit cell occupy the T2 and T1x sites, respectively (Table S10, ESI†). The reasonable thermal displacement parameters for the Li occupancies at T2 and T1x sites in addition to the decrease in R_{wp}, from 2.2 to 1.9%, are strong evidence of the existence of both of these sites in the Li_6PS_5Cl lattice structure (Tables S5–S7, ESI†).

In addition to the T5, T2, and T1x Li positions, the T5a Li position was also observed in Li_6PS_5Cl at 550 K according to the refinement results of the NPD data. At this temperature, about 3% of the total lithium atoms in the unit cell occupy the T5a site (Table S10, ESI†). While the T5a Li position is commonly reported in the argyrodite Li_6PS_5Br and Li_6PS_5I, it is not usually reported for Li_6PS_5Cl due to its relatively smaller lattice parameters. The observed T5a Li position at 550 K may be associated with the increased mobility of lithium ions and expanded lattice
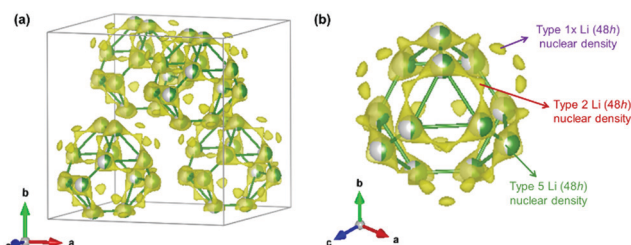

Fig. 3 (a) Overlap plot of Li atoms and Li nuclear density (equidensity level: 0.03 fm Å⁻³) of Li_6PS_5Cl in a unit cell. Li nuclear density results originate from the MEM analysis of NPD data collected at 300 K. (b) Illustration of the observed Li nuclear density distribution on type 2 Li (48h) and type 1x Li (48h) positions.
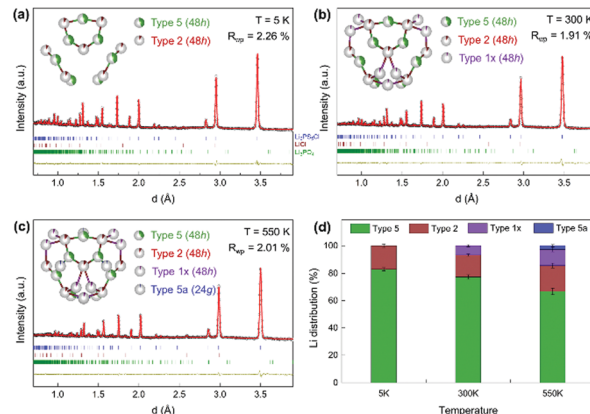
parameters at this higher temperature. At 5 K, Li mobility is highly limited, and the Li atoms preferentially occupy the lowest-energy lattice sites. As shown in Fig. 4a, only the T5 and T2 lattice sites of Li_6PS_5Cl are occupied, which suggests that the T5 and T2 sites are the low-energy positions for lithium ions (Table S4, ESI†). In addition, as presented in Fig. 4d, the degree of occupancy on the T1x and T5a sites increases with temperature, indicating that both of these sites correspond to higher energy positions, and occupation of these sites is possibly promoted by entropic contributions at higher temperatures. Since the site disorder between S^{2-} and Cl^- will not be affected by the temperature variation,[9,22] the consistent refinement results of the degree of site disorder at different temperatures confirm the reliability of the refinement process (Tables S4, S7 and S9, ESI†).

The in-depth understanding of Li distribution in the argyrodites Li_6PS_5Cl lattice can help provide additional insight into the lithium diffusion mechanisms of these systems. The T2 Li position was first noted by Deiseroth et al. and recently experimentally observed by Zeier et al.; T2 was demonstrated as a stable lattice site for Li location in Li_6PS_5Cl based on the above structure analysis.[10,22] Subsequent studies proposed that the T2 position is an intermediate site situated along the diffusion paths (considered as intra- and inter-cage hopping) in the conventional three-hop model.[17,22] The consideration of T2 site enabled a classification of possible Li diffusion pathways in the argyrodite lattice as follows: motion within a cage is possible via T5–T2–T5 (*intra-cage migration 1* shown in Fig. 5) and motion between two cages is possible via T5–T2–T2–T5 (*inter-cage migration 1* shown in Fig. 5).[17] When considering the role of the newly observed T1x site in the Li diffusion, another classification of possible Li diffusion pathway can be suggested: motion within a cage is possible via T5–T2–T1x–T2–T5 (*intra-cage migration 2* shown in Fig. 5) and motion between two cages is possible via T5–T2–T1x–T1x–T2–T5 (*inter-cage migration 2* shown in Fig. 5). In addition, the observed T5a Li position at high temperature indicates that, similar to Li_6PS_5Br and
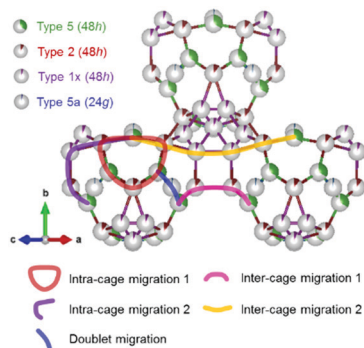
Fig. 5 Schematic structure of cage-like Li distribution in a Li_6PS_5Cl unit cell when T5, T2, T1x, and T5a Li positions are involved. The possible intra-cage, doublet, and inter-cage Li migration paths are illustrated using different colored lines.

Li_6PS_5I, the doublet Li migration in the argyrodites Li_6PS_5Cl lattice should also be considered (Fig. 5).[9,17]

In summary, using temperature-dependent NPD combined with MEM analysis, the Li distribution in the argyrodite Li_6PS_5Cl was studied. In addition to the previously reported T5 and T2 Li positions, a new Li lattice site (T1x) was observed in the Li_6PS_5Cl lattice. We propose that the role of this T1x Li position should be considered in the Li migration model of the argyrodite structure. These new insights regarding the Li distribution, as well as the newly proposed conduction pathways, provide a more complete description of the Li diffusion mechanisms in the argyrodite lattice compared to previous mechanistic models. This model deepens the understanding of the relationship between ionic diffusion and the Li sublattice structure, which will not only lead to the further optimization of existing argyrodite electrolytes, but also provide structural guidance for the design of new high-conductivity solid-state electrolytes.

Conflicts of interest

There are no conflicts to declare.

Notes and references

1 J. Janek and W. G. Zeier, *Nat. Energy*, 2016, **1**, 16141.
2 A. Banerjee, X. Wang, C. Fang, E. A. Wu and Y. S. Meng, *Chem. Rev.*, 2020, **120**, 6878–6933.
3 T. Famprikis, P. Canepa, J. A. Dawson, M. S. Islam and C. Masquelier, *Nat. Mater.*, 2019, **18**, 1278–1291.
4 R. Chen, Q. Li, X. Yu, L. Chen and H. Li, *Chem. Rev.*, 2020, **120**, 6820–6877.
5 M. A. Kraft, S. Ohno, T. Zinkevich, R. Koerver, S. P. Culver, T. Fuchs, A. Senyshyn, S. Indris, B. J. Morgan and W. G. Zeier, *J. Am. Chem. Soc.*, 2018, **140**, 16330–16339.
6 L. Zhou, A. Assoud, Q. Zhang, X. Wu and L. F. Nazar, *J. Am. Chem. Soc.*, 2019, **141**, 19002–19013.
7 H. J. Deiseroth, S. T. Kong, H. Eckert, J. Vannahme, C. Reiner, T. Zaiss and M. Schlosser, *Angew. Chem., Int. Ed.*, 2008, **47**, 755–758.
8 P. Adeli, J. D. Bazak, K. H. Park, I. Kochetkov, A. Huq, G. R. Goward and L. F. Nazar, *Angew. Chem., Int. Ed.*, 2019, **58**, 8681–8686.
9 M. A. Kraft, S. P. Culver, M. Calderon, F. Böcher, T. Krauskopf, A. Senyshyn, C. Dietrich, A. Zevalkink, J. R. Janek and W. G. Zeier, *J. Am. Chem. Soc.*, 2017, **139**, 10909–10918.
10 S. T. Kong, H. J. Deiseroth, C. Reiner, O. Gün, E. Neumann, C. Ritter and D. Zahn, *Chem. – Eur. J.*, 2010, **16**, 2198–2206.
11 N. J. J. de Klerk, I. Rosłoń and M. Wagemaker, *Chem. Mater.*, 2016, **28**, 7955–7963.
12 H.-J. Deiseroth, J. Maier, K. Weichert, V. Nickel, S. T. Kong and C. Reiner, *Z. Anorg. Allg. Chem.*, 2011, **637**, 1287–1294.
13 R. Schlem, M. Ghidiu, S. P. Culver, A.-L. Hansen and W. G. Zeier, *ACS Appl. Energy Mater.*, 2020, **3**, 9–18.
14 X. Feng, P.-H. Chien, Y. Wang, S. Patel, P. Wang, H. Liu, M. Immediato-Scuotto and Y.-Y. Hu, *Energy Storage Mater.*, 2020, **30**, 67–73.
15 I. Hanghofer, M. Brinek, S. L. Eisbacher, B. Bitschnau, M. Volck, V. Hennige, I. Hanzu, D. Rettenwander and H. M. R. Wilkening, *Phys. Chem. Chem. Phys.*, 2019, **21**, 8489–8507.
16 H. M. Chen, C. Maohua and S. Adams, *Phys. Chem. Chem. Phys.*, 2015, **17**, 16494–16506.
17 B. J. Morgan, *Chem. Mater.*, 2021, **33**, 2004–2018.
18 A. Baktash, J. C. Reid, T. Roman and D. J. Searles, *npj Comput. Mater.*, 2020, **6**, 162.
19 R. P. Rao and S. Adams, *Phys. Status Solidi A*, 2011, **208**, 1804.
20 O. Pecher, S. T. Kong, T. Goebel, V. Nickel, K. Weichert, C. Reiner, H. J. Deiseroth, J. Maier, F. Haarmann and D. Zahn, *Chem. – Eur. J.*, 2010, **16**, 8347–8354.
21 W. Huang, L. Cheng, S. Hori, K. Suzuki, M. Yonemura, M. Hirayama and R. Kanno, *Mater. Adv.*, 2020, **1**, 334–340.
22 N. Minafra, M. A. Kraft, T. Bernges, C. Li, R. Schlem, B. J. Morgan and W. G. Zeier, *Inorg. Chem.*, 2020, **59**, 11009–11019.
23 X. He, Y. Zhu and Y. Mo, *Nat. Commun.*, 2017, **8**, 15893.
24 F. Izumi and K. Momma, *IOP Conf. Ser.: Mater. Sci. Eng.*, 2011, **18**, 022001.
25 F. Izumi, *Solid State Ionics*, 2004, **172**, 1–6.
26 K. Momma, T. Ikeda, A. A. Belik and F. Izumi, *Powder Diffr.*, 2013, **28**, 184–193.
27 S. Song, D. Sheptyakov, A. M. Korsunsky, H. M. Duong and L. Lu, *Mater. Des.*, 2016, **93**, 232–237.
28 Y. Ren and X. Zuo, *Small Methods*, 2018, 1800064.
29 E. Zhao, Z. Zhang, X. Li, L. He, X. Yu, H. Li and F. Wang, *Chin. Phys. B*, 2020, **29**, 018201.